Structure–Activity Studies on Splitomicin Derivatives as Sirtuin Inhibitors and Computational Prediction of Binding Mode

Robert C. Neugebauer,[†] Urszula Uchiechowska,[‡] Rene Meier,[‡] Henning Hruby,[†] Vassil Valkov,[†] Eric Verdin,[§] Wolfgang Sippl,[‡] and Manfred Jung*,[†]

Institute of Pharmaceutical Sciences, Albert-Ludwigs-Universität Freiburg, Albertstr. 25, 79104 Freiburg, Germany, Department of Pharmaceutical Chemistry, Martin-Luther Universität Halle-Wittenberg, Wolfgang-Langenbeckstr. 4, 06120 Halle/Saale, Germany, and Gladstone Institute of Virology and Immunology, University of California, 1650 Owens Street, San Francisco, California 94158

Received August 6, 2007

NAD^+-dependent histone deacetylases (sirtuins) are enzymes that cleave acetyl groups from lysines in histones and other proteins. Potent selective sirtuin inhibitors are interesting tools for the investigation of the biological functions of those enzymes and may be future drugs for the treatment of cancer. Splitomicin was among the first two inhibitors that were discovered for yeast sirtuins but showed rather weak inhibition on human enzymes. We present detailed structure–activity relationships on splitomicin derivatives and their inhibition of recombinant Sirt2. To rationalize our experimental results, ligand docking followed by molecular mechanics Poisson–Boltzmann/surface area (MM-PBSA) calculations were carried out. These analyses suggested a molecular basis for the interaction of the beta-phenylsplitomicins with human Sirt2. Protein-based virtual screening resulted in the identification of a novel Sirt2 inhibitor chemotype. Selected inhibitors showed antiproliferative properties and tubulin hyperacetylation in MCF7 breast cancer cells and are promising candidates for further optimization as potential anticancer drugs.

Introduction

Histone deacetylases (HDACs[a]) are transcriptional regulators that deacetylate histones and various nonhistone proteins. This enzymatic activity is affecting the conformational state and the activities of the substrate–proteins.[1] Three classes of histone deacetylases have been described in humans: class I and II have been shown to be zinc-dependent amidohydrolases and 11 subtypes have been described (HDAC1−11). Class III enzymes rely in their catalysis on NAD^+ with the subsequent formation of nicotinamide and O-acetyl ADP ribose (Chart 1) as a result of the transacetylation. Based on the homology to the yeast histone deacetylase Sir2p, the NAD^+-dependent deacetylases have been termed sirtuins and seven members (Sirt1–7) have been identified in humans.[2]

Whereas class I and II histone HDACs have been identified as bona fide anticancer targets and clinical studies of their inhibitors as new anticancer agents are under way,[3] much less is known about the consequences of class III HDAC inhibition.[2] Sirtuins have been linked to aging and overexpression of sirtuins leads to a prolonged lifespan in yeast.[4] Lately, sirtuins activity has been tied to the pathogenesis of HIV[5] and cancer[6–8] and also neurological diseases.[9,10] Only a limited number of sirtuin inhibitors is known and some of them do not inhibit human subtypes.[11,12] The first synthetic inhibitor that was discovered is sirtinol (**1**;[13] Chart 1), but in certain cases, it has been shown that precipitation of the enzyme by the inhibitor contributes to the in vitro inhibition.[14] Structure–activity relationships of sirtinol analogues have been reported very recently.[15] Shortly after sirtinol, splitomicin (**2a**) was published as an inhibitor of yeast sirtuins[16] that is not active on human subtypes. Initial structure–activity relationships on **2a** have been described,[17,18] and for the first time selective inhibition of individual subtypes (here yeast enzymes) could be demonstrated. Compound **2b** (HR73) was introduced as another splitomicin derivative by us that was the first potent inhibitor (IC_{50} < 5 μM) of human isoforms[5] (see Chart 1). More inhibitors are available for Sirt2 that have been discovered using a virtual screening approach but cellular activity and verification of protein hyperacetylation has not been demonstrated.[19,20] Lately, indoles like **3** with activity down to around 0.1 μM have been presented.[21] The

Chart 1. Known Sirtuin Inhibitors

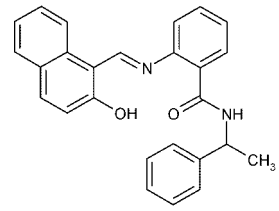

1

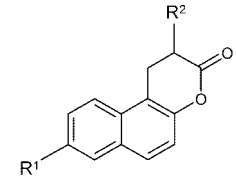

2a: R^1 = H; R^2 = H
2b: R^1 = Br; R^2 = phenyl

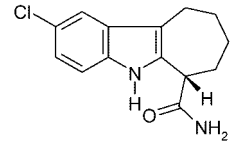

3

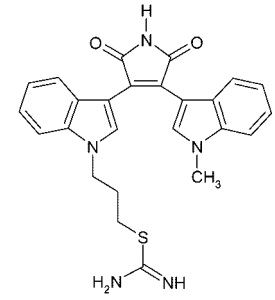

4

* To whom correspondence should be addressed. Tel.: +49-761-203-4896. Fax: +49-761-203-6321. E-mail: manfred.jung@pharmazie.uni-freiburg.de.

[†] Albert-Ludwigs-Universität Freiburg.

[‡] Martin-Luther Universität Halle-Wittenberg.

[§] University of California.

[a] Abbreviations: HDAC, histone deacetylase; MM-PBSA, molecular mechanics Poisson–Boltzmann/surface area; IPTG, isopropyl-β-D-thiogalactopyranosid; SAHA, suberoylanilide hydroxamic acid.

10.1021/jm700972e CCC: $40.75
Published on Web 02/13/2008

Scheme 1. Synthesis of β-Phenylsplitomicins by Friedel–Crafts Alkylation

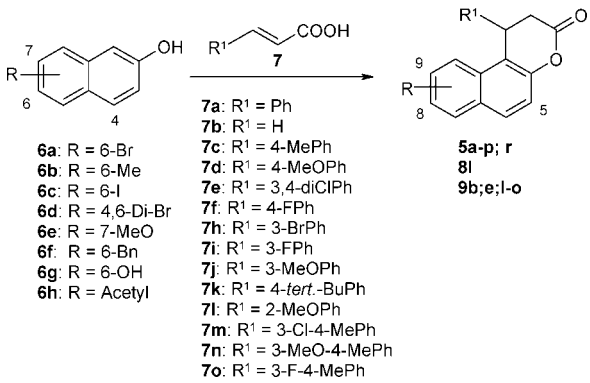

sirtuin inhibitor cambinol was discovered from random screening, and for the first time, anticancer activity in an animal model could be demonstrated using this compound.[22] Using a focused library screening approach, we had identified kinase inhibitors such as **4** (Ro-318220) as new lead structures for sirtuin inhibitors that target the adenosine binding pocket. By applying computational and competition experiments, we showed that these inhibitors target the adenosine binding pocket.[23] We set out to perform structure–activity studies on splitomicin derivatives and initial biological results led us to focus on β-aryl derivatives and Sirt2 inhibition. Selected compounds were tested for antiproliferative activity and for intracellular tubulin acetylation. To investigate the molecular interactions that are important in determining the inhibitory activity and also to clarify the spatial orientations that the splitomicins adopt within the Sirt2 binding pocket, a molecular modeling study was carried out. The newly synthesized β-phenylsplitomicins were first analyzed by an automated molecular docking (GOLD) followed by a molecular mechanics Poisson–Boltzmann/surface area (MM-PBSA)[24] analysis. Based on the docking and free energy calculations, we observed a clear preference for one of the two β-phenylsplitomicin stereoisomers. To experimentally verify the proposed binding mode, the enantiomers of two potent β-phenylsplitomicins were synthesized and tested. Furthermore, introducing new analogues of splitomicins identified by virtual screening, we were able to show that a lactam substitution of the lactone ring is well tolerated, provided that other features beneficial for strong sirtuin inhibition are retained. Because the lactam ring, unlike the lactone ring in splitomicin, is not expected to hydrolyze this suggests that splitomicins may act as reversible inhibitors and not as acetylating agents as had been postulated before.

Results and Discussion

Chemistry. The 8-bromo substituent in **2b** had been shown to be crucial for the activity against human sirtuins as compared to the unsubstituted congeners. Thus, we initially prepared a series of β-aryl-8-bromosplitomicins **5a**−**p** and **5r** by the acid-catalyzed cyclization of cinnamic acids **7a** and **7c**−**e** with β-naphthols **6a**−**h** (see Scheme 1 and Table 1). Similarly, the use of acrylic acid (**7b**) instead of a cinnamic acid led to the β-unsubstituted compound **5p**. As an 8-methyl group proved to be a good alternative to the 8-bromo-substituent (see below), we also prepared a series of splitomicins **8** starting from 6-methyl-2-naphthol **6b** or the α,β-unsaturated lactone **10b** by conjugate addition, respectively. Further use of 6-iodo-2-naphthol (**6c**), 4,6-dibromo-2-naphthol (**6d**), 7-methoxy-2-naphthol (**6e**), 6-benzyl-2-naphthol (**6f**), 2,6-dihydroxynaphthalene (**6g**), and 6-acetyl-2-naphthol (**6h**) led to a series of β-phenylsplitomicins **9** (see Scheme 1).

Table 1. Inhibition of Sirtuins by Splitomicin Derivatives

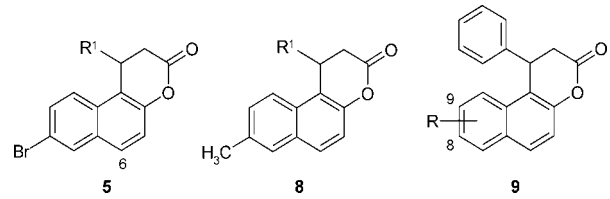

cmpd	substitution	Sirt2 (IC_{50} ± SE or inhibition at concentration, μM)
nicotinamide		32.3 ± 6.6
1		53.0 ± 15.8
5a	R^1: Ph	5.2 ± 1.0
5b	R^1: 4-ClPh	28.5 % @ 20
5c	R^1: 4-MePh	1.5 ± 0.5
5d	R^1: 4-MeOPh	5.4 ± 1.5
5e	R^1: 3,4-diClPh	42.3 % @ 20
5f	R^1: 4-FPh	7.9 ± 1.8
5g	R^1: 3,4-diFPh	19.7 ± 5.5
5h	R^1: 3-BrPh	10.1 ± 2.6
5i	R^1: 3-FPh	3.2 ± 0.8
5j	R^1: 3-MeOPh	2.3 ± 0.3
5k	R^1: 4-tert.-BuPh	46.8 % @ 20
5l	R^1: 2-MeO	17.4 % @ 20
5m	R^1: 3-Cl-4-MePh	2.3 ± 0.6
5n	R^1: 3-F-4-MePh	2.0 ± 0.7
5o	R^1: 3-MeO-4-MePh	6.3 % @ 20
5p	R^1: H	no inhib. @ 20
5q	R^1: Bn	21.1 % @ 40
5r	R^1: Ph; 6-Pos: Br	9.6 % @ 40
8a	R^1: Ph	10.6 ± 1.6
(*R*)-**8a**	R^1: Ph	3.4 ± 0.2
(*S*)-**8a**	R^1: Ph	41.8 % @ 100
8b	R^1: 4-ClPh	26.7 % @ 20
8c	R^1: 4-MePh	1.5 ± 0.6
(*R*)-**8c**	R^1: 4-MePh	1.0 ± 0.3
(*S*)-**8c**	R^1: 4-MePh	35.1 % @ 100
8d	R^1: 3-F-4-MePh	3.4 ± 0.3
8e	R^1: 3-MeO-4-MePh	9.2 % @ 20
8f	R^1: 3-CNPh	3.1 ± 0.5
8g	R^1: 3-$CONH_2$	20.0 ± 7.8
8h	R^1: 3-MePh	4.4 ± 0.6
8i	R^1: 3-HOPh	15.4 % @ 20
8j	R^1: 4-PhPh	28.3 % @ 20
8k	R^1: 3-$NHCOCH_3$Ph	17.1 % @ 20
8l	R^1: 3-BrPh	9.8 ± 1.2
9°	R: 8-Et	25.6 % @ 40
9b	R: 8-I	19.5 ± 9.7
9c	R: 8-CN	25.9 % @ 40
9d	R: 8-Ph	26.2 % @ 40
9e	R: 8-Bn	no inhib. @ 40
9f	R: 8-$CONH_2$	no inhib. @ 40
9g	R: 8-(3-Py)	18.4 % @ 20
9h	R: 8-(3-HOPh)	37.5 % @ 20
9i	R: 8-(3-$CH_3CONHPh$)	22.2 % @ 20
9j	R: 8-(4-PhPh)	20.6 % @ 20
9k	R: 8-(2-naphthyl)	15.1 % @ 20
9l	R: 9-MeO	no inhib. @ 40
9m	R: 8-HO	21.8 % @ 20
9n	R: 8- CH_3CO	24.0 % @ 20
9o	R: 8-H	49.1 % @ 40

The 8-methyl-dehydrosplitomicin (**10b**) was synthesized using propiolic acid as the alkylating agent, as reported before for 2-naphthol (see Scheme 2).[17] The palladium-catalyzed conjugate addition[25] of arylboronic acids served as an alternative route to β-arylsplitomicins. Addition of a Grignard reagent[26] led to a β-benzyl 8-bromosplitomicin **5q** (see Scheme 2 and Table 1).

As all derivatives of β-phenylsplitomicins synthesized so far were racemates, the respective enantiomers were prepared for

Scheme 2. β-Phenylsplitomicins via Conjugate Additions

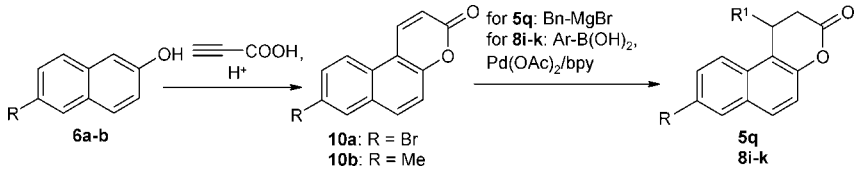

Scheme 3. Asymmetric Synthesis of β-Phenylsplitomicins

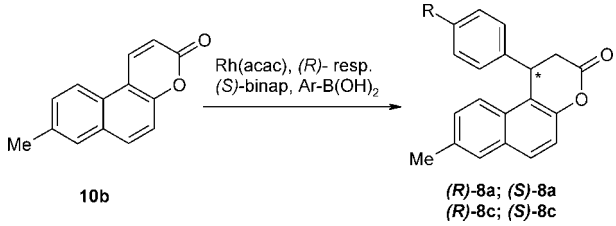

two potent β-phenyl-8-methyl-splitomicins applying an asymmetric conjugate addition protocol using a chiral rhodium catalyst[27] (see Scheme 3). According to the literature, the stereochemistry of the products can be assigned from the configuration of the catalyst used,[27] for example, the (*S*)-binap generates the (*S*)-arylsplitomicin.

The bromo substituent in the 8-position led to active sirtuin inhibitors, but also served as a useful starting point for structural variations via Pd-catalyzed couplings employing the β-aryl splitomicins as starting materials. Substituents introduced in the 8-position in this way were methyl-, ethyl-, phenyl-, 3-hydroxyphenyl-, biphenyl-, 2-naphthyl-, 3-pyridyl, 3-acetamidophenyl-, and cyano (see Scheme 4 and Table 1). For alkylgroups, alkylaluminium compounds served as the reagents,[28] for aryl groups, arylboronic acids under addition of fluoride[29] served as the reagents, and for the cyano group, zinc cyanide served as the reagent.[30] The cyano group in the 8- or the 3′-position of arylsplitomicins could be converted to a carboxamide function by mild palladium-catalyzed hydration, as described in the literature[31] (see Scheme 4).

Using a protein-based virtual screening approach (described in detail in Materials and Methods), we identified structurally related lactams in the Chembridge database and purchased and tested selected compounds **11a**−**d** for sirtuin inhibition as well (see Chart 2). As these compounds showed promising activity (see below), we also prepared a derivative **12** with a bromo substituent in the 8-position (see Scheme 5).

Enzyme Inhibition. All splitomicin derivatives were tested in initial studies for Sirt2 inhibition at concentrations of 20 and 40 μM in a homogeneous deacetylase assay using a fluorescent lysine derivative[14] that was developed in our group.[32] Usually, only if an inhibition of more than 50% at 40 μM or 20 μM was observed, IC_{50} determinations were performed. Nicotinamide and **1** were tested as reference compounds (see Table 1).

Depending on the substitution on the β-aryl ring, compounds that contain either a bromo or a methyl substituent in the 8-position can be sirtuin inhibitors with a potency in the low micromolar region, for example, a 4-methylphenyl group gives good inhibition in both series (**5c**, **8c**), whereas, for example, a 4-chlorophenyl substituent (**5b**, **8b**) or sterically demanding residues (**5k**, **8j**) leads to decreased inhibition. Additionally, polar moieties on the β-phenyl ring (**8g**, **8 h**, **8k**) diminish the inhibitory potency, but the cyano derivative **8f** shows good inhibition. Compounds **5m**−**o** were prepared as a consequence of the good inhibition of the compounds **5c**, **5i**, and **5j**, but no improvement was achieved. Compounds **5m** and **5n** inhibit Sirt2 also between 1 and 5 μM, whereas **5o** is inactive. For both **8a** and **8c**, the *R*-enantiomer is much more potent than the *S*-form.

Except for methyl, all other substituents in the 8-position (**9b**−**k**) or the 9-methoxy group in **9l** lead to a significant loss of activity. Commercially available compounds **11a**−**d** (see Chart 2) with a lactam structure instead of the lactone ring of splitomicin showed weak inhibitory potency. However, these compounds lack the 8-substituent that was shown to be necessary for good inhibition of human subtypes. They are considerably more active than the corresponding 8-unsubstituted lactone **9o** and, therefore, 8-substituted lactams seem to be an interesting target for further structure–activity-relationships. We have prepared one such compound, **12**, and it showed activity in the low micromolar region (Table 2). Originally, splitomicins were thought to be acylating inhibitors of sirtuins, and the reactivity toward hydrolysis had been correlated with enzyme–inhibitory potency.[17] While we cannot totally rule out such a mode of inhibition, our docking studies and SAR, especially with regard to the lactams, make this rather unlikely. Competition analysis showed that the most potent inhibitor (*R*)-**8c** is practically not competitive with respect to NAD^+ (see Supporting Information).

Docking Analysis. All Sirt2 structures contain a conserved 270 amino acid catalytic domain with variable N- and C-termini. The X-ray structures of several Sirt2 proteins have been published in the past few years, whereas no 3D structure is available for Sirt1.[33,34] The structure of the catalytic domain consists of a large classical Rossmann-fold and a small zinc binding domain. The interface between the large and the small subdomain is commonly subdivided into A, B, and C pocket. This division is based on the interaction of adenine (A), ribose (B) and nicotinamide (C), which are parts of the NAD^+ cofactor. Whereas the interaction of adenine and ribose is similar in all available sirtuin X-ray structures, the interaction of the nicotinamide part is less clearly defined. Several so-called productive and nonproductive conformations of nicotinamide have been observed in the crystal structures, reflecting the high flexibility of this part of the cofactor. In the X-ray structure of a Sirt2 homologue from Archeabacteria it was shown that the acetylated peptide binds in a cleft between the two domains. The acetyllysine residue inserts into a conserved hydrophobic pocket, where NAD^+ binds nearby. In the case of the human Sirt2 X-ray structure, which was crystallized as trimer, no structural information about the NAD^+ or substrate binding is available. However, due to the homology with bacterial sirtuins, it is obvious that the interaction of NAD^+ and substrate with Sirt2 is comparable with the bacterial X-ray structure complexes.

We have previously described the development of other series of Sirt2 inhibitors, including adenosine mimetics, for example, the bis-indolyl-maleimide **4**[23] and suramin derivatives.[35] Based on docking studies that we carried out for human Sirt2 and competition experiments with NAD^+, we found that the compounds interact with the adenine (for **4**) and the nicotinamide subpocket (suramin), respectively. Due to the structural dissimilarity between these inhibitors and the splitomicins, it can be expected that they interact in a different way with sirtuin

Scheme 4. Pd-Catalyzed Reactions on Splitomicin Derivatives

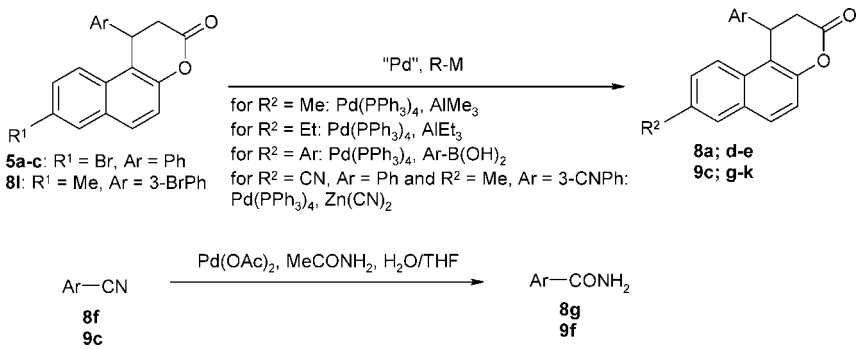

Chart 2. Lactam Analogues of Splitomicins

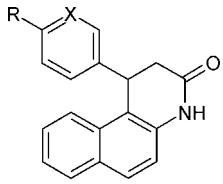

11a: R = H, X = CH
11b: R = F, X = CH
11c: R = H, X = N
11d: R = Ph, X = CH

Scheme 5. Synthesis of a Bromo-Substituted Lactam Analogue

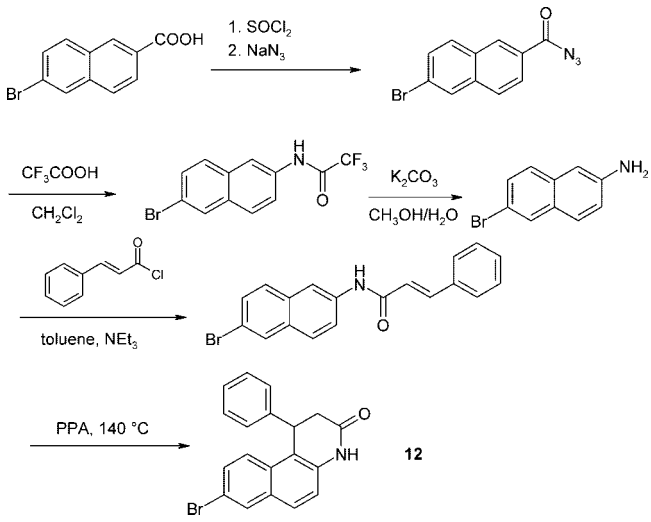

Table 2. Sirtuin Inhibition by the Compounds **11** (for Structures, see Chart *2*) and **12** (Scheme *5*)

cmpd	Sirt2 ($IC_{50} \pm$ SE or inhibition at concentration, μM)
11a	31.5% @ 40
11b	16.9% @ 40
11c	no inhib. @ 20
11d	4.2% @ 40
12	6.4 μM $\pm$ 0.3

proteins. In the present study, the X-ray structure of human Sirt2 was used for an automated ligand docking using the program GOLD.[36] A series of docking simulations were carried out to better rationalize the binding of the newly synthesized splitomicin derivatives. The analysis of the X-ray structure of human Sirt2 (which contains three monomers) and preliminary docking simulations using the known inhibitors cambinol and the indole **3** showed that the compounds interact with the nicotinamide subpocket (C) of Sirt2. The consideration of four water molecules found in all Sirt2 monomers, which are located at a narrow cavity nearby the active site, significantly improved the docking results. The polar moieties of known inhibitors, such as cambinol or **3**, were found to interact with the polar residues Gln167, Asn168, and the water molecules of the nicotinamide subpocket (for details, see Supporting Information). The β-phenylsplitomicins at first were prepared and tested as racemates, and therefore, both stereoisomers (*R* and *S*) were considered in the docking study. The obtained docking scores and the visual analysis of the docking poses showed that only the (*R*)-isomer is able to favorably interact with the nicotinamide subpocket (Figure 1a,b). All docked β-phenylsplitomicins showed the same binding mode, including a hydrogen bond to the water molecule bonded to Gln167 (Figure 2). The β-phenyl substituent of all (*R*)-isomers fits into a hydrophobic channel and is sandwiched between Phe119 and His187. This channel represents the binding site for the acetylated lysine residue of the substrate. For the (*S*)-enantiomers, the docking showed that the lactone ring is also facing toward the nicotinamide subpocket. However, no direct hydrogen bond was observed between (*S*)-**8a** and the residues of the active site (Figure 3a,b). Our proposed type of interaction of (*R*)-**8a** and (*R*)-**8c** with Sirt2 is similar to docking results recently published for other Sirt2 inhibitors.[9,19] Also, in these studies, polar moieties of the inhibitors were found to interact with the nicotinamide binding pocket C (Phe96, Gln167, Asn 168, Ile169).

Interaction possibilities at the binding pockets were analyzed by calculating the contact preferences using the MOE program. The purpose of this knowledge-based approach is to calculate preferred locations for hydrophobic ligand atoms from the 3D coordinates of the binding site. The visual analysis of the contact preferences further supported the binding mode obtained by the GOLD[36] docking (Figure 4a,b). The most favorable interaction with hydrophic ligand atoms was observed in the acetyl-lysine channel and nearby Tyr104 and Val233. The favored polar interactions were detected nearby the polar residues Gln167 and Asn168, which are in agreement with the location of the water molecules.

The docking study and the visual inspection of the interaction possibilities clearly suggested that the *R*-enantiomers represent the active form of the β-phenylsplitomicins, whereas for the *S*-enantiomer, no clear binding mode was observed. The experimental results showed that the *R*-enantiomers are more than two log units more active than the *S*-enantiomers, which is in perfect agreement with the docking results.

In the next step, we analyzed the obtained docking scores for all studied inhibitors. In the case of the enantiomers (*R*)-**8a**, (*S*)-**8a**, (*R*)-**8c**, and (*S*)-**8c**, higher scores were observed for the *R*-species. The docking results showed that the active inhibitors can interact in similar ways with the adenine-binding pocket.

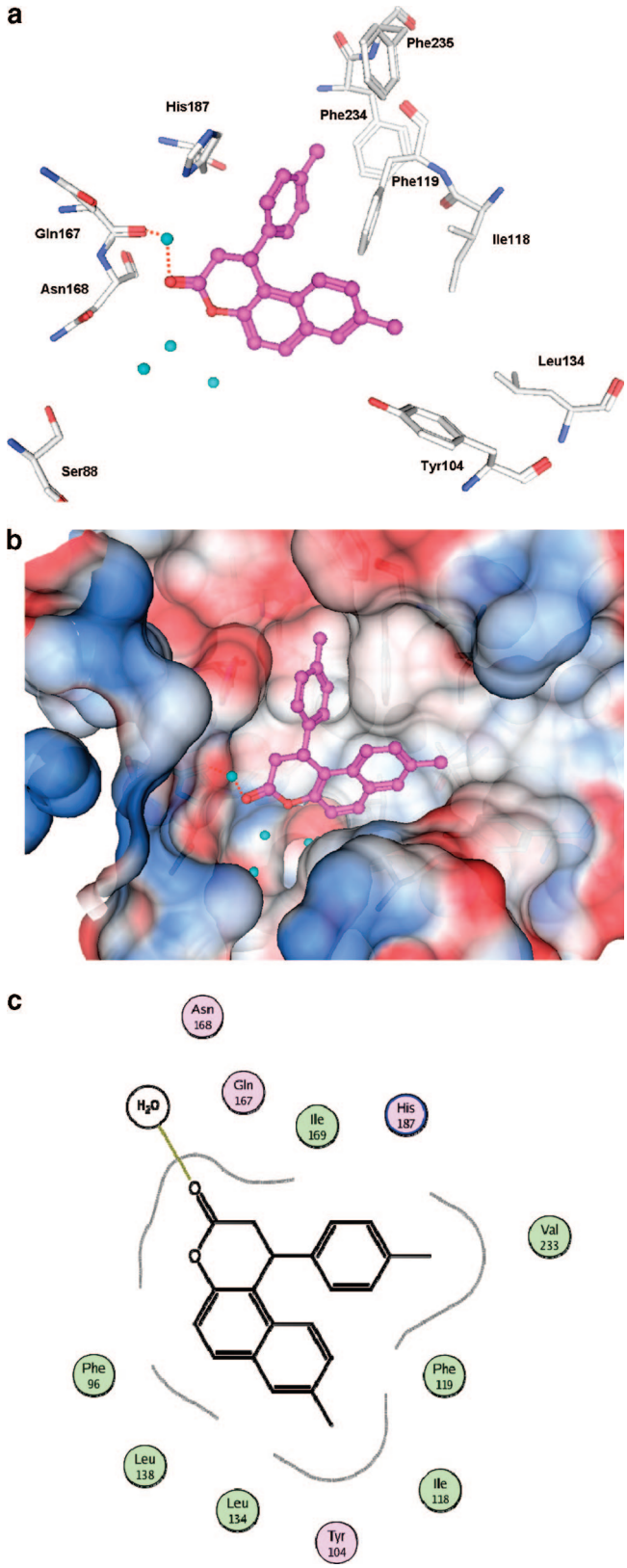

Figure 1. (a) Interaction of (*R*)-**8c** (magenta) with the amino acid residues of human Sirt2. The four water molecules used within the docking study are colored cyan. Hydrogen bonds are indicated by the red dashed line. (b) Interaction of (*R*)-**8c** (magenta) at the nicotinamide binding site. The Conolly molecular surface of the binding pocket is colored according the electrostatic potential (blue = positive potential, red = negative potential). (c) Schematic representation of the interaction between (*R*)-**8c** and human Sirt2. Hydrophobic amino acids are colored green, polar are colored purple. Hydrogen bonds are displayed as a dashed line.

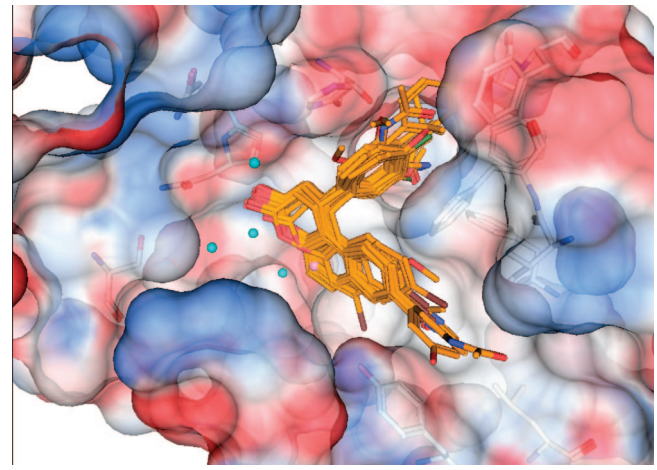

Figure 2. Docking solutions for the *R*-enantiomers of the active β-phenylsplitomicins (orange). The substituted β-phenyl rings of the inhibitors are all facing towards the acetyl-lysine binding channel. The Conolly molecular surface of the binding pocket is colored according to the electrostatic potential (blue = positive potential, red = negative potential).

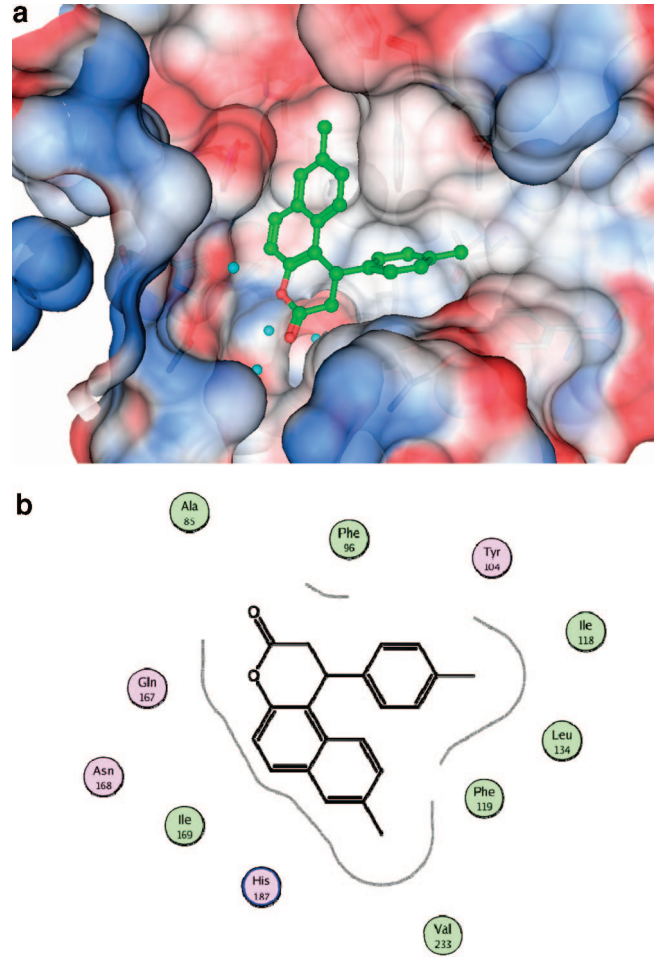

Figure 3. (a) Predicted binding mode of (*S*)-**8c** (green) at the nicotinamide binding site of human Sirt2. The four water molecules used within the docking study are colored cyan. The Conolly molecular surface of the binding pocket is colored according the electrostatic potential (blue = positive potential, red = negative potential). (b) Schematic representation of the interaction between (*S*)-**8c** and human Sirt2. Hydrophobic amino acids are colored green, polar are colored purple.

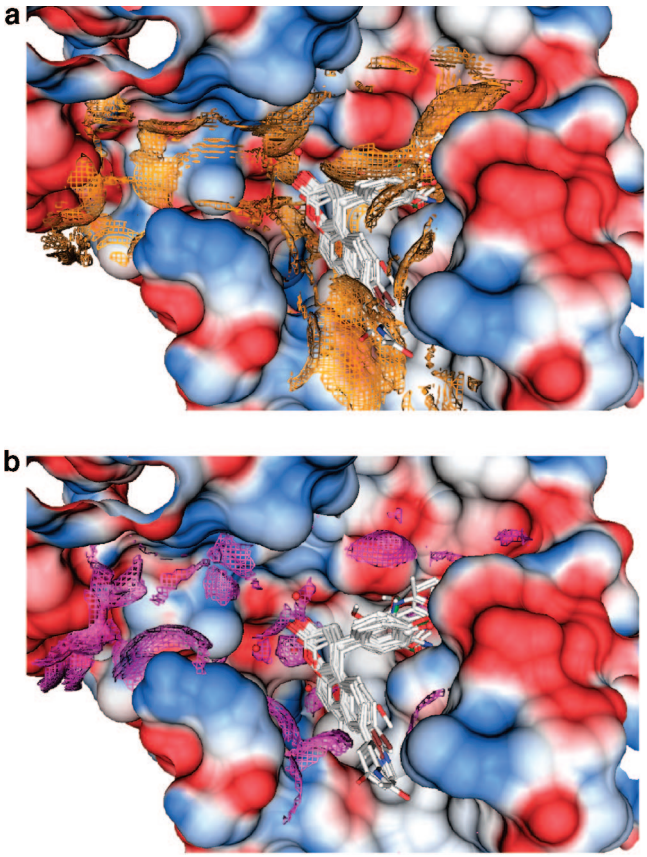

Figure 4. Interaction possibilities at the binding pocket, as analyzed by calculating the contact preferences using the MOE program. The docked inhibitors (*R*-enantiomers) are colored atom-type coded. The Conolly molecular surface of the binding pocket is colored according the electrostatic potential (blue = positive potential, red = negative potential). (a) The favourable hydrophobic contact preferences (contour level 90%) are colored orange. (b) The favourable hydrophilic contact preferences (contour level 90%) are colored magenta.

However, on the basis of the Goldscore values, no discrimination could be derived between more- and less-active splitomicin inhibitors. It is shown in many docking studies that often a low correlation is observed between docking scores and biological activities.[37] Therefore, we focused on a more accurate method for the analysis of key interactions necessary for strong inhibitory activity.

MM-PBSA Approach. To make a more precise and quantitative analysis of the protein inhibitor interaction, several Sirt2−splitomicin complexes were used as starting structures for MD simulations. These simulations showed that both kinds of complexes are stable during the 5 ns free MD simulation. The inhibitor interactions observed in the starting structures (obtained by means of GOLD) were generally maintained after the MD simulations. Analyzing the root-mean-square deviation (rmsd) from the complex structures of all of the heavy atoms of the proteins, the rmsd remained approximately constant around the range of 0.7–1.4 Å (for details, see Supporting Information).

Successively, the MD trajectories were further analyzed through the MM-PBSA method.[38–42] In the MM-PBSA method, the absolute free energy of a system is estimated from a combination of molecular mechanics energy, a Poisson–Boltzmann estimate of the electrostatic free energy, an estimate of the solvation free energy determined from the exposed surface area, and an estimate of the entropy of the molecule derived from a normal modes calculation. Because the inhibitors **8a** and **8c** were synthesized and tested as enantiomers, we focused our free energy calculations on this set of inhibitors.

Table 3. Cytotoxicity on MCF 7 Cells

cmpd	growth inhibition (GI_{50})
5c	43 μM
8c	99 μM
(*R*)-**8c**	84 μM
(*S*)-**8c**	74% at 500 μM
8g	64% at 500 μM
9d	57% at 500 μM

Table 4. Energy Contributions to the Free Energy of Binding as Obtained by the MM-PBSA Approach

	Sirt2/(*R*)-**8c**	Sirt2/(*S*)-**8c**	Sirt2/(*R*)-**8a**	Sirt2/(*S*)-**8a**
ΔE_{elect}	−7.81	−3.22	−2.09	−0.19
ΔE_{vdW}	−30.87	−31.54	−38.68	−31.44
ΔE_{gas} (ΔE_{elect} + ΔE_{vdW})	−38.68	−34.76	−40.77	−31.63
ΔG_{solv}	9.77	10.74	7.63	5.66
$T\Delta S_{tot}$	−21.50	−19.29	−25.79	−23.27
ΔG_{calcd}	−7.41	−4.73	−7.35	−2.7

The binding free energies for the two pairs of stereoisomers were estimated (Table 4) using the MM-PBSA method described in the Materials and Methods section. The calculated mean binding free energies were −7.41 kcal/mol for (*R*)-**8c** and −4.73 kcal/mol for (*S*)-**8c**, respectively. Also for **8a** the MM-PBSA calculation predicted the *R*-enantiomer to bind stronger to Sirt2 (*R*)-**8a**, −7.35 kcal/mol, vs (*S*)-**8a**, −2.70 kcal/mol. Thus, binding of (*R*)-**8c** is 2.68 kcal/mol more favorable than for the *S*-enantiomer, whereas in case of **8a** the energy difference is 4.65 kcal/mol. The estimated binding free energies are in good agreement with the biological data where the *S*-enantiomers are more than two log units less-active than the *R*-enantiomers ($\Delta\Delta G_{expt} > \sim 3$ kcal/mol, calculated on the basis of the IC_{50} values measured at 310 K). The detailed analysis of the hydrogen bonding during the MD simulation showed that the Sirt2/*R*-enantiomer complexes have more intermolecular hydrogen bonds stabilizing the complex than the complexes with the *S*-enantiomers (see Materials and Methods section).

Antiproliferative Activity. Selected inhibitors **5c**, **8c**, and both of its enantiomers, **8g** and **9d**, were tested for inhibition of proliferation of MCF-7 breast cancer cells using the 3-(4,5-dimethylthiazol-2-yl)-2,5-diphenyltetrazolium bromide (MTT) assay.[43] Generally, the splitomicins are not very potent cytotoxic agents on those cells. This may be due to their high lipophilicity. But those compounds that inhibited the enzyme in the low micromolar region (**5c**, **8c**, (*R*)-**8c**) were also the most potent antiproliferative agents. The weaker enyzme inhibitors showed some inhibition of cell growth, but even at 500 μM, no complete growth inhibition and, hence, no IC_{50} values could be obtained. (see Table 3).

Protein Hyperacetylation. To verify whether the inhibitors actually target the desired enzyme at concentrations where antiproliferative activity was observed, we analyzed tubulin acetylation by Western blot. Indeed, compounds **5c** and (*R*)-**8c** led to tubulin hyperacetylation consistent with Sirt2 inhibition. The Sirt2 inhibitor **3** and the HDAC class I/II-inhibitor SAHA, which is known to induce tubulin hyperacetylation via HDAC6[44,45] inhibition, were used as reference compounds (see Supporting Information). Taken together, the cellular data links anticancer activity to Sirt2 inhibition. It is interesting to note that the levels of tubulin hyperacetylation that can be reached using SAHA or similar inhibitors of zinc-dependent HDACs were never reached with any of the sirtuin inhibitors. This argues

for a larger contribution of tubulin acetylation maintenance by HDAC6 as compared to Sirt2.

Conclusion

Structure–activity relationships for β-aryl splitomicins led to the identification of Sirt2 inhibitors that are active in the low micromolar region. A link between increased enzyme inhibition and anticancer activity could be established. This supports the use of our fluorescent small molecule in sirtuin assays to identify antiproliferative agents. Docking studies confirmed that in the whole series of β-phenylsplitomicines the orientation of the β-phenyl group is important for their Sirt2 activity. Only in the case of the *R*-enantiomers of the chiral inhibitors the interaction with the substrate binding channel is observed. The preparation and biological testing of two pairs of enantiomers confirmed the docking results. Furthermore, we reported calculations of binding free energies between these two pairs of enantiomers and Sirt2 using the recently developed MM-PBSA method. This approach proved to be attractive for rationalizing at a quantitative manner the interaction of the splitomicines and Sirt2. The competition experiment carried out with NAD^+ clearly showed that the β-phenylsplitomicins are noncompetitve to the cofactor. The comparison of the predicted binding mode of (*R*)-**8a** and the observed interaction of NAD^+ in the homologous bacterial sirtuin X-ray structure complexes further supported the noncompetition between both molecules and is in agreement with recently published structural data on sirtuin homologues.[46] Further optimization of splitomicin-based sirtuin inhibitors and the novel lactam analogues, therefore, can now be performed in a more rational fashion.

Experimental Section

Materials and Methods. Standard chemicals were purchased from Sigma, Aldrich, or Lancaster. 3-Methoxy-4-methylbenzaldehyde was purchased from Frinton Laboratories (Vineland, NJ) and 3-Fluoro-4-methylcinnamic acid from Matrix Scientific (Columbia, SC). Compound **1** was purchased from Axxora (Lausen, Switzerland). Compound **2a**,[17] 6-methyl-2-naphthol (**6b**),[47] 6-iodo-2-naphthol (**6c**),[48] and 4,6-dibromo-2-naphthol (**6d**)[49] were prepared according to published procedures. Cinnamic acids **7c**−**e** were prepared from the corresponding benzaldehydes according to standard procedures. ^{1}H NMR spectra were obtained on a Bruker Avance DRX 400 MHz spectrometer, and ^{1}H chemical shifts are reported in ppm (δ). Merck Kieselgel 60 was used for flash chromatography with either cyclohexane/ethyl acetate mixtures or cyclohexane/dichloromethane mixtures as eluents so that the R_f value of the desired product was about 0.3. Absolute configurations of enantiomers were assigned from the stereochemistry of the catalysts according to the literature.[27] A CEM Discover was used as the microwave reactor.

Cyclization of Naphthols with Cinnamic and Acrylic Acids with Amberlyst 15, Method A. The β-naphthol (3 mmol), the cinnamic acid (6 mmol), and Amberlyst 15 ion-exchange resin (300 mg) were refluxed in toluene (15 mL) overnight. The resin was filtered off and washed with toluene. The solvent was removed under reduced pressure. Separation by column chromatography led to the isolation of the splitomicins.

Method B for Deactivated Cinnamic Acids. The naphthol (3 mmol), the deactivated cinnamic acid (6 mmol), and 100 μL of sulfuric acid were refluxed in toluene (15 mL) overnight. After cooling, the reaction mixture was washed twice with aqueous sodium carbonate solution. The organic phases were collected and dried over sodium sulfate, and the solvent was removed under reduced pressure. Separation by column chromatography yielded the desired products.

Conjugate Addition of Boronic Acids, Method C. To a Schlenk tube, aryl boronic acid (3.0 mmol), α,β-unsaturated lactone **10b** (1.0 mmol), $Pd(OAc)_2$ (0.050 mmol), 2,2′-bipyridine (0.20 mmol), acetic acid (1.0 mL), THF (0.5 mL), and water (0.3 mL) were added under nitrogen. The mixture was stirred and heated at 40 °C for three days and then neutralized with saturated sodium bicarbonate solution and extracted with diethyl ether. The combined ether solution was washed with brine, dried (sodium sulfate), and concentrated. The residue was purified by column chromatography to give splitomicins.

Asymmetric Conjugate Addition of Boronic Acids, Method D. A solution of $Rh(acac)(C_2H_4)_2$ (9.0 μmol), chiral ligand ((*R*)- and (*S*)-binap, respectively; 9.9 μmol), α,β-unsaturated lactone **10b** (0.30 mmol), and boronic acid (3.0 mmol) in a mixture of 1,4-dioxane (1.0 mL) and water (0.1 mL) were placed in a sealed tube under nitrogen and stirred at 60 °C for 14 h. Then the solution was passed through a short pad of silica gel with *tert*-butylmethylether as eluent. The solvent was removed under reduced pressure, and the resulting residue was purified by column chromatography, furnishing the desired product.

Pd-Catalyzed Introduction of a Methyl Group, Method E. The bromo-substituted splitomicin derivative (0.50 mmol), trimethylaluminium (0.50 mmol), and tetrakis(triphenylphospine)palladium (0.025 mmol) in dry 1,4-dioxane were refluxed for 2 h. After cooling, the reaction mixture was diluted with water. The product was extracted with dichloromethane and then purified by column chromatography on silica gel.

Microwave-Accelerated Suzuki Coupling, Method F. To a stirred mixture of arylboronic acid (0.90 mmol), bromo-substituted splitomicin derivative (0.60 mmol), and powdered CsF (1.80 mmol) in a mixture of dry methanol (1.5 mL) and dimethoxyethane (3.0 mL) was added tetrakis(triphenylphospine)palladium(0) (27 μmol). The reaction mixture was flushed with nitrogen, sealed, and placed in a microwave field (100 W) for 8 min. Subsequent filtration and purification by column chromatography afforded the desired product.

Pd-Catalyzed Aromatic Cyanation, Method G. The bromo-substituted splitomicin derivative (0.30 mmol) is combined with zinc cyanide (0.18 mmol) and tetrakis(triphenylphospine)palladium(0) (7.2 μmol) in deoxygenated DMF (2.5 mL), and the yellow slurry was heated to 80 °C under nitrogen. Then the mixture was cooled down to room temperature, diluted with toluene (10 mL), and washed twice with 5% sodium bicarbonate solution. The organic layer was collected, washed with brine, and concentrated under reduced pressure to provide the product, which was purified by column chromatography on silica gel.

Pd-Catalyzed Hydration of Nitriles to Amides, Method H. The cyano-substituted splitomicin derivative (0.5 mmol) was dissolved in a mixture of THF (0.8 mL) and water (0.2 mL). Acetamide (2.0 mmol) and $Pd(OAc)_2$ (0.05 mmol) were added, and the mixture was strirred at room temperature for 6 h. Then the solvents were removed under reduced pressure and the residue was subjected to column chromatography to yield the amide.

Synthesis of Inhibitors. The compounds were synthesized using the above-mentioned methods and general methods for organic syntheses. They were analyzed for identity and purity using IR, MS, ^{1}H and ^{13}C NMR, and elemental analyses or HPLC. Enantiomeric excess was determined using HPLC. The details are given in the Supporting Information (^{13}C NMR data not shown). Analytical data for three selected compounds is listed below.

8-Bromo-1-phenyl-1,2-dihydro-benzo[*f*]chromen-3-one (5a). By method A, yield = 201 mg (19%) as a white solid. ^{1}H NMR ($CDCl_3$): 8.02 (d, J = 2.0 Hz, 1H, 7-H), 7.77 (d, J = 9.0 Hz, 1H, 10-H), 7.65 (d, J = 9.0 Hz, 1H, 6-H), 7.52 (dd, J_1 = 9.0 Hz, J_2 = 2.0 Hz, 1H, 9-H), 7.29 (d, J = 9.0 Hz, 1H, 5-H), 7.29–7.20 (m, 3H, Ph-H), 7.10–7.08 (m, 2H, Ph-H), 4.91 (dd, J_1 = 6.7 Hz, J_2 = 2.4 Hz, 1H, 1-H), 3.22 (dd, J_1 = 15.7 Hz, J_2 = 6.7 Hz, 1H, 2-H), 3.15 (dd, J_1 = 15.7 Hz, J_2 = 2.4 Hz, 1H, 2-H).

8-Methyl-1-(4-methylphenyl)-1,2-dihydro-benzo[*f*]chromen-3-one (8c). By method E, using **5c** as the bromo-substituted splitomicin derivative, yield = 113 mg (75%) as a white solid. ^{1}H NMR ($CDCl_3$): 7.79 (d, J = 8.9 Hz, 1H, 10-H), 7.71 (d, J = 8.6 Hz, 1H, 6-H), 7.65 (s, 1H, 7-H), 7.33 (d, J = 8.9 Hz, 1H, 9-H),

7.32 (d, $J = 8.6$ Hz, 1H, 5-H), 7.09 (d, $J = 8.2$ Hz, 2H, Ph-H), 7.02 (d, $J = 8.2$ Hz, 2H, Ph-H), 4.92 (dd, $J_1 = 2.2$ Hz, $J_2 = 6.6$ Hz, 1H, 1-H), 3.20 (dd, $J_1 = 6.6$ Hz, $J_2 = 15.7$ Hz, 1H, 2-H), 3.15 (dd, $J_1 = 15.7$ Hz, $J_2 = 2.2$ Hz, 1H, 2-H), 2.48 (s, 3H, CH_3-Np), 2.28 (s, 3H, CH_3-Ph).

(*R*)-8-Methyl-1-(4-methylphenyl)-1,2-dihydro-benzo[*f*]chromen-3-one ((*R*)-8c). By method D, using **10b** as α,β-unsaturated splitomicin derivative, (*R*)-binap as chiral ligand, and *p*-tolyl boronic acid, yield = 16 mg (18%) as a white solid; ee = 98.9%, as determined by chiral HPLC. $[\alpha]_{589} = 11.3°$ ($c = 1.0$ mg/mL, CH_2Cl_2, $T = 20$ °C); for ^{1}H NMR data, see **8c**.

Recombinant Proteins. Human Sirt2 (N-terminally tagged with 6 His) was prepared as described previously,[50] with minor modifications. In brief, the plasmid pEV1440, containing the full-length human Sirt2 cDNA, was transformed in *E. coli* strain BL21 for expression. The culture is grown in LB media to an optical density of 0.6 (A_{600}) at 37 °C, induced with 0.1 mM IPTG for 2 h, and pelleted. Lysis is performed using a French press. The soluble overexpressed recombinant protein was purified using Ni-NTA resin. The identity of the produced His-Sirt2 was verified using SDS electrophoresis. Deacetylase activity of the produced Sirt2 was dependent on NAD^+ and could be inhibited with sirtinol and nicotinamide.

Fluorescent Deacetylase Assay. All compounds were evaluated for their ability to inhibit recombinant sirtuins using a homogeneous fluorescent deacetylase assay.[32] Stock solutions of inhibitors were prepared in DMSO, and 3 μL or less of a suited DMSO inhibitor solution were added to the incubation mixture. The assay was carried out in 96-well plates: 60 μL reaction volume contained the fluorescent histone deacetylase substrate ZMAL (10.5 μM), NAD^+ (500 μM), and Sirt2 (3 μL). After 4 h of incubation at 37 °C, the deacetylation reaction was stopped and the formed metabolite ZML (deacetylated form of ZMAL) was developed using a tryptic digest to form a fluorophor. Then, fluorescence was measured in a plate reader (BMG Polarstar) with a coumarin filter (excitation 390 nm and emission 460 nm). The amount of remaining substrate in the positive control with inhibitor versus negative control without inhibitor was employed to calculate inhibition. All determinations were at least carried out in duplicate. IC_{50} data were analyzed using GraphPad Prism Software.

Cytotoxicity Assays. MCF-7 human breast tumor cells were obtained from Max-Delbrück-Centre of Molecular Medicine (Berlin) and maintained in RPMI-1640 supplemented with 10% fetal bovine serum, 1% 2 mM L-glutamine, and 1% penicillin/streptomycin (Invitrogen). The cells were incubated at 37 °C in an atmosphere of 5% CO_2. Cells were seeded at 5000 per well in 100 μL of growing medium in 96-well tissue culture plates. At 24 h after seeding, diluted compounds or DMSO vehicle control were added to each well and incubated for 72 h at 37 °C. Growth inhibition was determined using the MTT assay. Data was plotted as the percentage of DMSO-treated control against compound concentration using GraphPad Prism 4.0. The 50% growth inhibition (GI_{50}) was calculated as the compound concentration required to reduce cell number by 50% compared with control.

Western Blot. Cells were seeded at 500000 per well in 6-well tissue culture plates. At 24 h after seeding, cells were treated with diluted compounds or DMSO and incubated for 8 h at 37 °C. The cells were washed with PBS and lysed in 50 mM Tris-HCl, pH 7.5, 0.5 mM EDTA, 150 mM NaCl, 0.5% NP-40, 1× complete protease inhibitors (Roche, Germany). Protein concentration was determined with BCA protein assay kit (Pierce). For Western blot analysis, protein samples were separated in 30% SDS-PAGE gels and blotted onto ImmobilonP membrane (Millipore). Membranes were blocked with Roti-Block (Roth) and probed with antiacetylated α-tubulin (6-11B1; Sigma) and anti α-tubulin (B-5-1-2; Sigma). ECL detection (Pierce) was performed according to manufacturer's instructions.

Computational Details. All calculations were performed on a Pentium IV 1.8/2.2 GHz based Linux cluster (20 CPUs). The molecular structures of the inhibitors were generated using the MOE modeling package (Chemical Computing Group). The structures were energy minimized using the MMFF94s force field and the conjugate gradient method, until the default derivative convergence criterion of 0.01 kcal/(mol × Å) was met. The crystal structure of human Sirt2 (pdb code 1J8F) was taken from the Protein Data Bank. Sirt2 is a monomer in solution and, therefore, only the chain B was chosen from the trimeric Sirt2 structure of 1J8F. As in our recent docking study,[23] monomer B of Sirt2 was selected, as it showed the best stereochemical quality examined with the program PROCHECK. Because the X-ray structures might contain a strain from the crystallization process, the Sirt2 structure was first energy minimized. After adding all hydrogen atoms, including all water molecules, a descent minimization was carried out on the Sirt2 structure using the MMF94 force field and the GB/SA continuum[51] solvent model for water. During the minimization, a tethering constant of 100 kcal/(mol × Å) on the backbone atoms was applied, after a stepwise reduction of the tethering to 1 kcal/(mol × Å).

Inhibitor Docking. Docking of the newly synthesized inhibitors was carried out using program GOLD 3.0[36] and the minimized native human Sirt2 structure. This approach has been shown to be successful for ligand docking by us[35,52] and others.[20] All torsion angles in each inhibitor were allowed to rotate freely. The binding site was defined on Ile169 with an radius of 15 Å. Goldscore was chosen as fitness function due to the success in former docking studies on sirtuins.[23] For each molecule, 10 docking runs were performed. The resulting solutions were clustered on the basis of the heavy atom rmsd values (1 Å). The top-ranked poses for each ligand were retained and analyzed graphically within MOE 2006.08 (Chemical Computing Group).[53] Interaction possibilities at the binding pockets were analyzed by calculating the contact preferences using the MOE program. The purpose of this knowledge-based approach is to calculate, from the 3D coordinates of the binding site, preferred locations for hydrophobic ligand atoms. The calculation was carried out on the solvent stripped X-ray strucutre of Sirt2 (1j8f, chain B). The calculated polar and hydrophobic contact preferences were then viewed superimposed on the crystal structure and homology models using the MOE program. The Conolly molecular surface of the binding pocket was calculated using the MOE program and colored according the molecular electrostatic potential (using MMF94 charges within MOE). The conformation of the binding mode of NAD^+ was taken from our former docking studies of sirtuin ligands.[23,35]

Virtual Screening. We screened the Chembridge database for inhibitors structurally related to the β-phenylsplitomicins. The compounds of the Chembridge database were transformed into 3D molecular structures using the Omega module from OpenEye Software.[54] The ∼328000 molecules were stored in a MOE database (Chemical Computing Group) and ESshape3D MOE fingerprints were calculated. The ESShape3D is an eigenvalue spectrum shape fingerprint. Each fingerprint is a fixed length and allows for comparison of 3D shapes made from the heavy atoms of a molecule. Compounds similar to **8a** (with an inverse distance > 0.9) were retrieved and further analyzed. Among the retrieved compounds 17 lactam analogs of **8a** were identified. The lactams were docked into the human Sirt2 protein structure using the GOLD program and the same settings as described above. GoldScores were calculated for all docking poses that were subsequently visually analyzed within MOE. To confirm the virtual screening results, four lactam analogs of **8a** that showed a similar binding mode as the β-phenylsplitomicins were selected and purchased from Chembridge.

MD Simulations. Molecular dynamics (MD) and thermodynamic computations were carried out using Amber 9.0[38] and the Amber1999SB force field.[55] We focused our MD simulations on the two pairs of separated stereoisomers **8a** and **8c**. The initial structure of the four Sirt2-inhibitor complexes were taken from the GOLD docking study. The ligand force field parameters were taken from the general Amber force field (GAFF),[56] whereas AM1 ESP atomic partial charges were assigned to the inhibitors.[57] In the crystal structure of human Sirt2, each domain is associated with a divalent zinc ion coordinated to four anionic cystein side groups.

The divalent zinc ions were represented by a cationic dummy atom (CaDA) approach of Pang et al.,[24,58] which treats the zinc ion as a tetrahedron-shaped divalent cation with dummy atoms filling the tetrahedral corners. Parameters and libraries for the tetrahedral-zinc groups and anionic cystein residues were obtained from Pang et al.[24,58,59] An explicit solvent model TIP3P water was used, and the complexes were solvated with a 10 Å water cap. A total of eight sodium ions were added as counterions to neutralize the system. Prior to the free MD simulations, three steps of relaxation were carried out; in the first step, we kept the protein fixed with a constraint of 500 kcal $mol^{-1}Å^{-1}$, and we relaxed the position of the tetrahedron-shaped zinc cations (0.1 ps MD). In the second step, the zinc divalent cations and the inhibitor structures were relaxed for 0.5 ps, during which the protein atoms were restrained to the X-ray coordinates with a force constant of 500 kcal $mol^{-1}Å^{-1}$. In the final step, all restraints were removed and the complexes were relaxed for 1 ps. The temperature of the relaxed system was then equilibrated at 300 K through 20 ps of MD using 2 fs time steps. A constant volume periodic boundary was set to equilibrate the temperature of the system by the Langevin dynamics[39] using a collision frequency of 10 ps^{-1} and a velocity limit of 5 temperature units. During the temperature equilibration routine, the complex in the sovent box was restrained to the initial coordinates with a weak force constant of 10 kcal $mol^{-1}Å^{-1}$. The final coordinates of the temperature equilibration routine (after 20 ps) was then used to complete a 1 ns molecular dynamics routine using 2 fs time steps, during which the temperature was kept at 300 K by the Langevin dynamics[39] using a collision frequency of 1 ps^{-1} and a velocity limit of 20 temperature units, and the pressure of the solvated system was equilibrated at 1 bar at a certain density in a constant pressure periodic boundary by an isotropic pressure scaling method employing a pressure relaxation time of 2 ps. The time step of the free MD simulations was 2 fs, with a cutoff of 9 Å for the nonbonded interaction, and SHAKE[55] was employed to keep all bonds involving hydrogen atoms rigid. Electrostatic interactions were computed using the Particle Mesh Ewald method.[40] The MD simulations of the Sirt2-inhibitor complexes were performed in total for 6 ns.

MM-PBSA. The net change in binding free energy accompanying the formation of the protein–ligand complex is approximated by the following equation

$$\Delta G = \Delta H - T\Delta S \tag{1}$$

in which T is the temperature of the system at 300 Kelvin. The binding free energy (ΔG) of the protein–ligand complex is computed as:

$$\Delta G = G_{complex} - [G_{protein} + G_{ligand}] \tag{2}$$

where $G_{complex}$ is the absolute free energy of the complex, $G_{protein}$ is the absolute free energy of the protein, and G_{ligand} is the absolute free energy of the ligand. We extracted 100 snapshots (at time intervals of 2 ps) for each species (complex, protein, and ligand) from the last 200 ps of the MD simulations of the complexes. The enthalpy term in eq 1 is dissected into subenergy terms

$$H_{tot} = H_{gas} + G_{solv} \tag{3}$$

$$H_{gas} = E_{el} + E_{vdW} + E_{int} \tag{4}$$

where H_{gas} is the potential energy of the solute, which is determined as the sum of van der Waals (E_{vdw}), electrostatic (E_{el}), and internal energies (E_{int}) in gas phase by using the SANDER module of Amber.[38] G_{solv} is the solvation free energy for transferring the solute from vacuum into solvent and is a sum of electrostatic (G_{el}) and nonelectrostatic (hydrophobic) contributions (G_{nonel}), as shown in eq 5

$$G_{solv} = G_{el} + G_{nonel} \tag{5}$$

G_{el} in eq 4 was computed at 0.15 M salt concentration by the PBSA module of Amber 9.0 by dividing implicitely solvated solute species into 0.4 Å cubic grid points and summing up the electrostatic potentials computed at each grid point. Electrostatic potential $Ø_{(r)}$ at a grid point r, which is not at the solvent–solute boundary, was computed by a linear Poisson–Boltzmann (PB) equation,[38] which is a three-dimensional vector differential equation as in eq 6

$$\nabla\epsilon_{(r)}\nabla Ø_{(r)} = -4\pi \times \rho(r) \tag{6}$$

in which $\epsilon_{(r)}$ is the dielectric constant ($\epsilon = 1$ for the solute interior and $\epsilon = 80$ for implicit PB water) and $\rho_{(r)}$ is the charge density. The grid point potentials were then summed up for each atom i to yield atomic potentials $Ø_i$. The PB implicit solvent molecules at the solute–solvent boundary were allowed to energetically converge over 1000 iterations before the single-point Poisson computations were implemented by PBSA for each snapshot. A spherical solvent probe (radii) of 1.4 Å and atomic radii provided by the Amber force field were used for the implicit solvent molecules and solute atoms, respectively, during the PBSA computations.

The absolute entropy was computed for each solute species by normal-mode analysis[60] integrated in the NMODE module of Amber 9.0. The total entropy (S_{tot}), as formulated in eq 7, arose from changes in the degree

$$S_{tot} = S_{trans} + S_{rot} + S_{vib} \tag{7}$$

of freedom [translational (S_{trans}), rotational (S_{rot}), and vibrational (S_{vib})] of each species.[42]

Considering all absolute energy terms as given in eq 2, the binding free energy ΔG takes the following form

$$\Delta G_{binding} = [\Delta H_{gas} + \Delta G_{solv}] - T\Delta S_{tot} \tag{8}$$

Parameter/topology files used in MM-PBSA computations were prepared for the complex, the protein, and the inhibitors using the LEAP module. Snapshots extracted from trajectories were preminimized in the gas phase by the SANDER module using a conjugate gradient method until the root-mean-square-deviation of the elements of the gradient vector was less than 10^{-4} kcal/$mol^{-1}Å^{-1}$. Frequencies of the vibrational modes were computed at 300 K for these minimized structures, including all snapshot atoms and using a harmonic approximation of the energies.[42]

Hydrogen Bond Analyses. A comprehensive hydrogen bond analyses was carried out on the trajectory of the splitomicin−Sirt2 complexes. Watson–Crick base pair formation and intermolecular protein−inhibitor interactions contributing to the specificity of binding was characterized by analyzing hydrogen bond formations through the trajectory of 6 ns MD simulation. A solvation pattern for bound isomeres was also characterized by hydrogen bond formation for the last 5 ns of the 6 ns simulation, during which all water molecules are thought to be pre-equilibrated. A cutoff distance of 3 Å between the heavy atoms of donor and acceptor groups and a hydrogen bonding angle cutoff of 120° was used to analyze hydrogen bond formation. Intermolecular hydrogen bond occurrence >1% was only found for the *R*-isomer (Gln167 and Ile169, 2.85% and 4.23%). A solvation pattern (water molecules) for this stereoisomer was found with 17.44% occurrence. For the *S*-isomer, only a solvation pattern with an occurrence of 11.25% was observed throughout the 5 ns period.

Acknowledgment. Funding by the Deutsche Forschungsgemeinschaft (Ju295-4/1 and -4/2, Si868/1-1) is gratefully acknowledged.

Supporting Information Available: Spectral data for newly synthesized compounds, inhibitor competition analysis, Western blot and data on compound purity, and data on the binding mode analysis. This material is available free of charge via the Internet at http://pubs.acs.org.

References

(1) Grozinger, C. M.; Schreiber, S. L. Deacetylase enzymes: Biological functions and the use of small-molecule inhibitors. *Chem. Biol.* **2002**, *9*, 3–16.
(2) North, B. J.; Verdin, E. Sirtuins: Sir2-related NAD-dependent protein deacetylases. *Genome Biol.* **2004**, *5*, 224.
(3) Johnstone, R. W. Histone-deacetylase inhibitors: novel drugs for the treatment of cancer. *Nat. Rev. Drug Discovery* **2002**, *1*, 287–299.

(4) Imai, S.; Armstrong, C. M.; Kaeberlein, M.; Guarente, L. Transcriptional silencing and longevity protein Sir2 is an NAD- dependent histone deacetylase. *Nature* **2000**, *403*, 795–800.

(5) Pagans, S.; Pedal, A.; North, B. J.; Kaehlcke, K.; Marshall, B. L.; Dorr, A.; Hetzer-Egger, C.; Henklein, P.; Frye, R.; McBurney, M. W.; Hruby, H.; Jung, M.; Verdin, E.; Ott, M. SIRT1 regulates HIV transcription via Tat deacetylation. *PLoS Biol.* **2005**, *3*, e41.

(6) Vaziri, H.; Dessain, S. K.; Ng Eaton, E.; Imai, S. I.; Frye, R. A.; Pandita, T. K.; Guarente, L.; Weinberg, R. A. hSIR2(SIRT1) functions as an NAD-dependent p53 deacetylase. *Cell* **2001**, *107*, 149–159.

(7) Bereshchenko, O. R.; Gu, W.; Dalla-Favera, R. Acetylation inactivates the transcriptional repressor BCL6. *Nat. Genet.* **2002**, *32*, 606–613.

(8) Ota, H.; Tokunaga, E.; Chang, K.; Hikasa, M.; Iijima, K.; Eto, M.; Kozaki, K.; Akishita, M.; Ouchi, Y.; Kaneki, M. Sirt1 inhibitor, Sirtinol, induces senescence-like growth arrest with attenuated Ras-MAPK signaling in human cancer cells. *Oncogene* **2005**.

(9) Outeiro, T. F.; Kontopoulos, E.; Altman, S.; Kufareva, I.; Strathearn, K. E.; Amore, A. M.; Volk, C. B.; Maxwell, M. M.; Rochet, J. C.; McLean, P. J.; Young, A. B.; Abagyan, R.; Feany, M. B.; Hyman, B. T.; Kazantsev, A. Sirtuin 2 inhibitors rescue {alpha}-synuclein-mediated toxicity in models of Parkinson's disease. *Science* **2007**, *317*, 516–519.

(10) Garske, A. L.; Smith, B. C.; Denu, J. M. Linking SIRT2 to Parkinson's disease. *ACS Chem. Biol.* **2007**, *2*, 529–532.

(11) Schäfer, S.; Jung, M. Chromatin modifications as targets for new anticancer drugs. *Arch. Pharm. Chem. Life Sci.* **2005**, *338*, 347–357.

(12) Biel, M.; Wascholowski, V.; Giannis, A. Epigenetics−An epicenter of gene regulation: Histones and histone-modifying enzymes. *Angew. Chem., Int. Ed.* **2005**, *44*, 3186–3216.

(13) Grozinger, C. M.; Chao, E. D.; Blackwell, H. E.; Moazed, D.; Schreiber, S. L. Identification of a class of small molecule inhibitors of the sirtuin family of NAD-dependent deacetylases by phenotypic screening. *J. Biol. Chem.* **2001**, *276*, 38837–38843.

(14) Heltweg, B.; Dequiedt, F.; Verdin, E.; Jung, M. A nonisotopic substrate for assaying both human zinc and NAD^+-dependent histone deacetylases. *Anal. Biochem.* **2003**, *319*, 42–48.

(15) Mai, A.; Massa, S.; Lavu, S.; Pezzi, R.; Simeoni, S.; Ragno, R.; Mariotti, F. R.; Chiani, F.; Camilloni, G.; Sinclair, D. A. Design, synthesis, and biological evaluation of sirtinol analogues as class III histone/protein deacetylase (sirtuin) inhibitors. *J. Med. Chem.* **2005**, *48*, 7789–7795.

(16) Bedalov, A.; Gatbonton, T.; Irvine, W. P.; Gottschling, D. E.; Simon, J. A. Identification of a small molecule inhibitor of Sir2p. *Proc. Natl. Acad. Sci. U.S.A.* **2001**, *98*, 15113–15118.

(17) Posakony, J.; Hirao, M.; Stevens, S.; Simon, J. A.; Bedalov, A. Inhibitors of Sir2: Evaluation of splitomicin analogues. *J. Med. Chem.* **2004**, *47*, 2635–2644.

(18) Hirao, M.; Posakony, J.; Nelson, M.; Hruby, H.; Jung, M.; Simon, J. A.; Bedalov, A. Identification of selective inhibitors of NAD^+-dependent deacetylases using phenotypic screens in yeast. *J. Biol. Chem.* **2003**, *278*, 52773–52782.

(19) Tervo, A. J.; Kyrylenko, S.; Niskanen, P.; Salminen, A.; Leppanen, J.; Nyronen, T. H.; Jarvinen, T.; Poso, A. An in silico approach to discovering novel inhibitors of human sirtuin type 2. *J. Med. Chem.* **2004**, *47*, 6292–6298.

(20) Tervo, A. J.; Suuronen, T.; Kyrylenko, S.; Kuusisto, E.; Kiviranta, P. H.; Salminen, A.; Leppanen, J.; Poso, A. Discovering inhibitors of human sirtuin type 2: Novel structural scaffolds. *J. Med. Chem.* **2006**, *49*, 7239–7241.

(21) Napper, A. D.; Hixon, J.; McDonagh, T.; Keavey, K.; Pons, J. F.; Barker, J.; Yau, W. T.; Amouzegh, P.; Flegg, A.; Hamelin, E.; Thomas, R. J.; Kates, M.; Jones, S.; Navia, M. A.; Saunders, J. O.; DiStefano, P. S.; Curtis, R. Discovery of indoles as potent and selective inhibitors of the deacetylase SIRT1. *J. Med. Chem.* **2005**, *48*, 8045–8054.

(22) Heltweg, B.; Gatbonton, T.; Schuler, A. D.; Posakony, J.; Li, H.; Goehle, S.; Kollipara, R.; Depinho, R. A.; Gu, Y.; Simon, J. A.; Bedalov, A. Antitumor activity of a small-molecule inhibitor of human silent information regulator 2 enzymes. *Cancer Res.* **2006**, *66*, 4368–4377.

(23) Trapp, J.; Jochum, A.; Meier, R.; Saunders, L.; Marshall, B.; Kunick, C.; Verdin, E.; Goekjian, P. G.; Sippl, W.; Jung, M. Adenosine mimetics as inhibitors of NAD^+-dependent histone deacetylases, from kinase to sirtuin inhibition. *J. Med. Chem.* **2006**, *49*, 7307–7316.

(24) Pang, Y. P. Novel zinc protein molecular dynamics simulations: Steps toward antiangiogenesis for cancer treatment. *J. Mol. Model.* **1999**, *5*, 196–202.

(25) Lu, X. Y.; Lin, S. H. Pd(II)-bipyridine catalyzed conjugate addition of arylboronic acid to α,β-unsaturated carbonyl compounds. *J. Org. Chem.* **2005**, *70*, 9651–9653.

(26) Abouassali, M.; Decoret, C.; Royer, J.; Dreux, J. Study on reactivity of coumarins. 1. Regioselectivity of Grignard reagents with coumarin. *Tetrahedron* **1976**, *32*, 1655–1659.

(27) Hayashi, T. Rhodium-catalyzed asymmetric addition of aryl- and alkenylboron reagents to electron-deficient olefins. *Pure Appl. Chem.* **2004**, *76*, 465–475.

(28) Ohta, A.; Inoue, A.; Watanabe, T. Introduction of the methyl group into the pyrazine ring. *Heterocycles* **1984**, *22*, 2317–2321.

(29) Wright, S. W.; Hageman, D. L.; Mcclure, L. D. Fluoride-mediated boronic acid coupling reactions. *J. Org. Chem.* **1994**, *59*, 6095–6097.

(30) Tschaen, D. M.; Desmond, R.; King, A. O.; Fortin, M. C.; Pipik, B.; King, S.; Verhoeven, T. R. An improved procedure of aromatic cyanation. *Synth. Commun.* **1994**, *24*, 887–890.

(31) Maffioli, S. I.; Marzorati, E.; Marazzi, A. Mild and reversible dehydration of primary amides with $PdCl_2$ in aqueous acetonitrile. *Org. Lett.* **2005**, *7*, 5237–5239.

(32) Heltweg, B.; Trapp, J.; Jung, M. In vitro assays for the determination of histone deacetylase activity. *Methods* **2005**, *36*, 332–337.

(33) Avalos, J. L.; Bever, K. M.; Wolberger, C. Mechanism of sirtuin inhibition by nicotinamide: Altering the NAD(+) cosubstrate specificity of a Sir2 enzyme. *Mol. Cell* **2005**, *17*, 855–868.

(34) Finnin, M. S.; Donigian, J. R.; Pavletich, N. P. Structure of the histone deacetylase SIRT2. *Nat. Struct. Biol.* **2001**, *8*, 621–625.

(35) Trapp, J.; Meier, R.; Hongwiset, D.; Kassack, M. U.; Sippl, W.; Jung, M. Structure−activity studies on suramin analogues as inhibitors of NAD(+)-dependent histone deacetylases (sirtuins). *ChemMedChem* **2007**, *2*, 1419–1431.

(36) Jones, G.; Willet, P.; Glen, R. C.; Leach, A. R.; Taylor, R. Development and validation of a genetic algorithm for flexible docking. *J. Mol. Biol.* **1997**, *267*, 727–748.

(37) Tame, J. R. Scoring functions—The first 100 years. *J. Comput.-Aided Mol. Des.* **2005**, *19*, 445–451.

(38) Case, D. A.; Cheatham, T. E. I.; Darden, T.; Gohlke, H.; Luo, R.; Merz, K. M. J.; Onufriev, A.; Simmerling, C.; Wang, W.; Woods, R. The Amber biomolecular simulation programs. *J. Comput. Chem.* **2005**, *26*, 1668–1688.

(39) Pastor, R. W.; Brooks, B. R.; Szabo, A. An analysis of the accuracy of Langevin and molecular dynamics algorithms. *Mol. Phys.* **1988**, *65*, 1409–1419.

(40) Darden, T.; Pedersen, L. Particle mesh Ewald: An Nlog(N) method for Ewald sums in large systems. *J. Chem. Phys.* **1993**, *103*, 8577–8593.

(41) Ryckaert, J. P.; Ciccotti, G.; Berendsen, H. J. C. Numerical integration of the cartesian equations of motions of a system with constraints: Molecular dynamics of *n*-alkanes. *J. Comput. Phys.* **1977**, *23*, 327–341.

(42) Gohlke, H.; Case, D. A. Converging free energy estimates: MM-PB(GB)SA studies on the protein−protein complex Ras−Raf. *J. Comput. Chem.* **2004**, *25*, 238–250.

(43) Mossman, T. Rapid colorimetric assay for cellular growth and survival: application to proliferation and cytotoxic assays. *J. Immunol. Methods* **1983**, *65*, 55–63.

(44) Hubbert, C.; Guardiola, A. R.; Shao, R.; Kawaguchi, Y.; Ito, A.; Nixon, A.; Yoshida, M.; Wang, X. F.; Yao, T. P. HDAC6 is a microtubule-associated deacetylase. *Nature* **2002**, *417*, 455–458.

(45) Zhang, Y.; Li, N.; Caron, C.; Matthias, G.; Hess, D.; Khochbin, S.; Matthias, P. HDAC-6 interacts with and deacetylates tubulin and microtubules in vivo. *EMBO J.* **2003**, *22*, 1168–1179.

(46) Sanders, B. D.; Zhao, K.; Slama, J. T.; Marmorstein, R. Structural basis for nicotinamide inhibition and base exchange in Sir2 enzymes. *Mol. Cell* **2007**, *25*, 463–472.

(47) Utley, J. H. P.; Rozenberg, G. G. Electroorganic reactions. Part 56: Anodic oxidation of 2-methyl- and 2-benzylnaphthalenes: Factors influencing competing pathways. *Tetrahedron* **2002**, *58*, 5251–5265.

(48) Smith, W. B. Some Observations on the iodination of 2-naphthol and its methyl ether. *J. Org. Chem.* **1985**, *50*, 3649–3651.

(49) Fries, H.; Schimmelschmidt, I. Darstellung von dibromnaphthol aus tribromnaphthol. *Justus Liebigs Ann. Chem.* **1930**, *484*, 245–271.

(50) North, B. J.; Schwer, B.; Ahuja, N.; Marshall, B.; Verdin, E. Preparation of enzymatically active recombinant class III protein deacetylases. *Methods* **2005**, *36*, 338–345.

(51) Still, W. C.; Tempczyk, A.; Hawley, R. C.; Hendrickson, T. Semianalytical treatment of solvation for molecular mechanics and dynamics. *J. Am. Chem. Soc.* **1990**, *112*, 6127–6129.

(52) Trapp, J.; Jung, M. The role of NAD^+ dependent histone deacetylases (sirtuins) in aging. *Curr. Drug Targets* **2006**, *7*, 1553–1560.

(53) *Molecular Operating Environment (MOE) 2006.8*; Chemical Computing Group Inc.: Montreal, Quebec, Canada, 2006.

(54) *Omega*; OpenEye Scientific Software: Santa Fe, NM, http://www.eyesopen.com.

(55) Hornak, V.; Abel, R.; Okur, A.; Strockbine, B.; Roitberg, A.; Simmerling, C. Comparison of multiple Amber force fields and development of improved protein backbone parameters. *Proteins* **2006**, *65*, 712–725.

(56) Wang, J.; Wolf, R. M.; Caldwell, J. W.; Kollman, P. A.; Case, D. A. Development and testing of a general amber force field. *J. Comput. Chem.* **2004**, *25*, 1157–1174.

(57) Wang, J.; Wang, W.; Kollman, P. A.; Case, D. A. Automatic atom type and bond type perception in molecular mechanical calculations. *J. Mol. Graph. Model.* **2006**, *25*, 247–260.
(58) Pang, Y. P.; Xu, K.; Yazal, J. E.; Prendergas, F. G. Successful molecular dynamics simulation of the zinc-bound farnesyltransferase using the cationic dummy atom approach. *Protein Sci.* **2000**, *9*, 1857–1865.
(59) Pang, Y. P. http://mayoresearch.mayo.edu/mayo/research/camdl/zinc_protein.cfm.
(60) Case, D. A. Molecular dynamics and normal mode analysis of biomolecular rigidity. *Rigidity Theory and Applications*; Plenum: New York, 1999; pp 329–344.

JM700972E